Elastic-Plastic Stress Analysis of Shrink-fitted Thick FGM Cylinders

Samiha Zrinej
Modeling of mechanical structures and systems
ENSAM of Rabat
Mohammed V University, Rabat
Morocco

Nor-Eddine Laghzale
Modeling of mechanical structures and systems
ENSAM of Rabat
Mohammed V University, Rabat
Morocco

Abdel-Hakim A. Bouzid
Mechanical Engineering Department
Ecole de Technologie Supérieure
Quebec, Canada

This paper addresses the stress analysis of shrink-fitted thick-walled cylinders made of functionally graded material (FGM). Analytical solutions are provided for the elastic-plastic behavior of shrink-fitted axisymmetric thick-walled FGM cylinders based on the linear plane elasticity theory and plasticity laws. Due to the material's functional gradation, mechanical characteristics like Young's modulus, yield stress, and plastic parameters are controlled by a power function along the wall thickness. Considering a plane strain case, elastic-perfectly plastic model and Von Mises yield criterion; theoretical solutions are obtained for both elastic and plastic phases. The radial, hoop, axial, and equivalent Von Mises stresses are obtained for up to 25%, 50%, and 75% of cylinder plasticization for the elastic and plastic zones. Stresses are given in terms of interference and geometrical and mechanical parameters of the assembly. In addition, the interferences to start plastic deformation and the full plastic collapse of the cylinder are discussed. Moreover, the effect of the gradient index on the contact pressure and both the start of yield and plastic collapse pressures are conducted. The analytical results found in the current research are compared with the numerical solutions carried out by Ansys Workbench. Both results show a good agreement.

Keywords: *Functionally graded material, Shrink-fit assembly, Interference, Von Mises's yield criterion, Plasticity, Ludwik hardening law, Graded-index, FEM.*

1. INTRODUCTION

Functionally Graded Materials (FGMs) are a unique class of composite materials that possess varying mate–rial properties in a desired direction or orientation. Their tailored material properties make them very appealing for use in various applications, including the potential reduction of stresses through thickness, improved thermal properties, higher fracture toughness, reduced stress intensity factors [1], and the stability of structures. Research studies in aerospace engineering have focused on the stability of plates and shells made from com–posite materials and honeycomb structures [2-5]. FGMs are increasingly used in cutting-edge sectors that require high performances, notably aerospace [6], automotive, tooling cat, biomedical, electronics, nuc–lear, and oil and gas sectors. Fully graded materials are attractive when optimizing pressure vessels and other structures. Because of their change of properties with the geometry, they have the capacity to reinforce the structure where required. For example, in pressure ves–sels, a higher strength is required at the inner diameter of cylinders where the stresses are high. The main application is high-pressure vessels and gun barrels, where new materials coupled to the autofrettage process are employed to increase the capacity to withhold higher pressures. High torque transmission, such as in ship propellers, is also another application. Miscellaneous methods have been used to investigate the analysis of FGM thick-walled cylinders subjected to mechanical and/or thermal loading using various approaches and assumptions. Shi et al. treated two types of hetero–geneous elastic hollow cylinders: multi-layer and conti–nuously graded materials. A method is developed to find the exact solution for N-layered FGM cylinders under uniform pressures, while a displacement method is used for continuously graded materials. The results are compared with numerical and reference counter–parts, and the inherent properties are discussed [7].

The elastic-plastic analysis for functionally graded thick-walled tubes subjected to internal pressure was investigated by Libiao Xin et al. using the rule-of-mixture with a function of radius to describe thermo-mechanical parameters of an FGM cylinder [8]. Bezzie et al. explored the impact of a graded index on the elastic responses of an axisymmetric pressurized and heated thick-walled functionally graded material (FGM) cylinder under plane strain conditions [9]. Nayak et al. investigated the propagation of the elastic-plastic front of a functionally graded rotating disk under centrifugal and thermal loads in the post-elastic regime. They have used a power law variation of the volume fraction, Hankey's deformation theory of plasticity, and Von Mises yield criteria to solve the displacement field [10]. On the other hand, the use of shrink-fit assemblies is growing for designing composite tubes, high-pressure vessels, nuclear reactors, and tank barrels [11]. This technique involves cooling down a smaller cylinder to fit into a larger cylinder, which then expands and pre–sses against each other. The strength of the connection

Received: March 2024, Accepted: May 2024
Correspondence to: Zrinej Samiha
ENSAM Rabat, Riad Toulal 2,
N 384 Meknes, Morroco
E-mail: chaltoutsamiha@gmail.com
doi: 10.5937/fme2403371Z

depends on the contact pressure and friction coefficient between the two surfaces. Proper design and manu–facturing are crucial for achieving the desired func–tionality. Numerous studies have been carried out using experiments and semi-analytical, analytical, and nume–rical methods. The majority of research has focused on one of two things: they either analyze the torque trans–mission capacity as a function of interference, or they optimize the design to minimize manufacturing costs and weight. In 2020, An analytical formulation for shrink-fitted axisymmetric thick-walled FGM cylinders using linear plane elasticity theory was conducted [12]. The effect of radial interference on the torque capacity of press-and shrink-fit gears has been investigated using finite element analysis in order to determine the static and dynamic coefficient of friction and address exce–ssive interference to prevent gear radial deformation [13]. The influence of radial interference on the torque capacity of shrink-fit camshafts was a similar topic that was covered by J. Zhao et al. in 2019 [14]; the results are anticipated for shrink-fit camshaft design and pro–duction. Mouâa et al. presented an analytical model for describing stresses and strain in a shrink-fit plastically deformed assembly under creep [15]. Also, Xiang-Fa Wu et al. investigated the stress and displacement fields in multiple shrink-fitted elastic cylinders under thermal and mechanical loads. The problem comes down to the evaluation of the interface pressures of neighboring tubes using tridiagonal linear algebraic equations [16]. In 2018, Kazemzadeh et al. explored the impact of shrink-fitting on the design of pressurized multi-layer composite tubes. It provides analytical solutions for structural response calculations and employs a nume–rical evolutionary optimization algorithm for weight and cost minimization. The results demonstrate the fact that the shrink-fitting parameters can lead to more econo–mical or lightweight assemblies, especially in cases with higher internal-to-external pressure ratios [17]. In addition to all the foregoing studies, many focused on shrink-fit FGM assemblies using shafts that remain in the elastic domain. However, few of these studies were carried out on plastic behavior. In this work, the inter–ferences that start yield and cause plastic collapse in an FGM shrink-fitted assembly were examined for various nonhomogeneity coefficients. Additionally, the residual pressure and stresses in the elastic and plastic zones were assessed for various nonhomogeneity coefficients. In order to evaluate and confirm the reliability of the precise solution, the results of the analytical model are contrasted with those of their FEM counterparts.

2. THEORETICAL ANALYSIS

Consider a shrink-fitted assembly of an FGM hollow cylinder of inner and outer radii, Ri and Ro, respec–tively, and an FGM hollow cylinder of inner and outer radii, r_i and r_0 respectively, as shown in the schematics of the FGM shrink-fitted cylinders in Fig.1. The prob–lem studied in cylindrical coordinates (r, θ, z). It is assumed that the FGM cylinders have a constant Poison's ratio and that they undergo a plastic defor–mation under plane strain (ε_z = 0) [18]. Figure 1 gives the geometry characteristics of the joint before assembly.

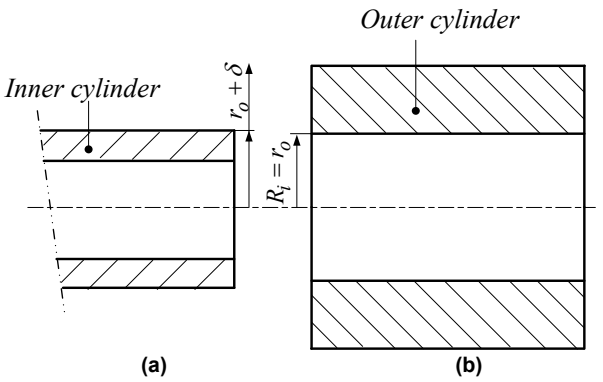

Figure 1. Joint before assembly

Young's modulus E and the yield stress σ_y are considered to vary with the radius according to the power-law expressed by (1) and (2).

For inner cylinder

$$E_s(r) = E_o\left(\frac{r}{r_i}\right)^e \tag{1}$$

$$\sigma_{ys}(r) = \sigma_{os}\left(\frac{r}{r_i}\right)^s \tag{2}$$

For outer cylinder

$$E_c(r) = E_0\left(\frac{r}{R_i}\right)^e \tag{3}$$

$$\sigma_{yc}(r) = \sigma_{oc}\left(\frac{r}{R_i}\right)^s \tag{4}$$

where E_0, σ_{os}, σ_{oc} are the reference values of E and σ_y, respectively, at the inner radius of the inner and outer cylinder, and e, s are gradient indexes. An elastic-plastic relationship with a power law strain hardening describes the behavior of the material model, expressed as follows:

$$\sigma_{eq}(r) = E(r)\varepsilon_{eq} \quad \left(if\ \sigma_{eq} \le \sigma_y\right) \tag{5}$$

$$\sigma_{eq}(r) = A(r) + B(r)\varepsilon_{eq}^m \quad \left(if\ \sigma_{eq} \ge \sigma_y\right) \tag{6}$$

where $A(r)$ and $B(r)$ are the Ludwick yield and work-hardening coefficient, respectively, which are power functions of the radius given respectively by (7) and (8) below, and m is the strain-hardening exponent.

$$A(r) = A_a\left(\frac{r}{R_i}\right)^n \tag{7}$$

$$B(r) = B_a\left(\frac{r}{R_i}\right)^k \tag{8}$$

where A_a and B_a are the reference values of Ludwik plastic parameters $A(r)$ and $B(r)$ obtained at the inside radius respectively, n and k are the gradient parameters.

When it comes to FGM materials, depending on the geometric and mechanical characteristics, the plastic deformation can start in the inner or outer cylinders or in both at the same time. In this article, we assume that only the outer cylinder undergoes elastoplastic deformation.

3. STRESS ANALYSIS

3.1 Elastic Analysis

As the interference increases, the deformation of the shrink-fit assembly is initially purely elastic.

The expression of the interference can be determined by considering the geometrical compatibility of the radial displacements:

$$\delta = u_r\left(R_i\right) - u_r\left(r_o\right) \tag{9}$$

The radial of the outer cylinder is given by [19]

$$u_r\left(R_i\right) = \frac{r_o}{Y_c^{\frac{\gamma}{2}} - Y_c^{\frac{-\gamma}{2}}}\left[\frac{Y_c^{-\frac{\gamma}{2}}}{A} - \frac{Y_c^{\frac{\gamma}{2}}}{B}\right]\frac{P_c}{E_b} \tag{10}$$

and that of the inner cylinder

$$u_r\left(r_o\right) = -\frac{r_o\, Y_s^{-e}}{Y_s^{\frac{\gamma}{2}} - Y_s^{\frac{-\gamma}{2}}}\left[\frac{Y_s^{\frac{\gamma}{2}}}{A} - \frac{Y_s^{\frac{-\gamma}{2}}}{B}\right]\frac{P_c}{E_b} \tag{11}$$

with

$$\begin{cases} A = (e-\gamma)(\nu-1) + 2\nu \\ B = (e+\gamma)(\nu-1) + 2\nu \end{cases} \tag{12}$$

where $Y_s = \frac{r_o}{r_i}$ and $Y_c = \frac{R_o}{R_i}$ are the ratios between the outer and inner radius of the inner and outer cylinders, respectively. γ and E_b are given by

$$\gamma = -\sqrt{\frac{e^2 + 4 - \nu(2+e)^2}{1-\nu}} \tag{13}$$

$$E_b = \frac{E_o}{2(1+\nu)(1-2\nu)} \tag{14}$$

E_b is a constant depending on the mechanical para–meters of the material. Substituting (10) and (11) into (9) gives:

$$\delta = \frac{r_o\, P_c}{E_b}\left[\begin{array}{l} \frac{1}{A}\left(\frac{1}{Y_c^{\gamma}-1} + \frac{Y_s^{\gamma-e}}{Y_s^{\gamma}-1}\right) \\ \qquad -\frac{1}{B}\left(\frac{1}{1-Y_c^{-\gamma}} + \frac{Y_s^{-e}}{Y_s^{\gamma}-1}\right) \end{array}\right] \tag{15}$$

The contact pressure is given by

$$P_c = \frac{\delta}{K} \tag{16}$$

where K is a function of the geometrical and mechanical parameters of the assembly.

$$K = \frac{r_o}{E_b}\left[\begin{array}{l} \frac{1}{A}\left(\frac{1}{Y_c^{\gamma}-1} + \frac{Y_s^{\gamma-e}}{Y_s^{\gamma}-1}\right) \\ \qquad -\frac{1}{B}\left(\frac{1}{1-Y_c^{-\gamma}} + \frac{Y_s^{-e}}{Y_s^{\gamma}-1}\right) \end{array}\right] \tag{17}$$

The contact pressure dependent on δ and K exp–ressed as a function of the geometrical and mechanical parameters of the assembly. The stresses in the radial, tangential and longitudinal directions are given hereafter for a plain strain.

For the inner cylinder $(r_i \le r \le r_0)$, the stress field is :

$$\sigma_r{}^s(r) = \frac{\left(\frac{r}{r_o}\right)^{\frac{e}{2}-1}}{Y_s^{\frac{\gamma}{2}} - Y_s^{\frac{-\gamma}{2}}}\left(\left(\frac{r}{r_i}\right)^{\frac{-\gamma}{2}} - \left(\frac{r}{r_i}\right)^{\frac{\gamma}{2}}\right)\frac{\delta}{\mathrm{K}} \tag{18}$$

$$\sigma_\theta{}^s(r) = \frac{1}{2}\frac{\left(\frac{r}{r_o}\right)^{\frac{e}{2}-1}}{Y_s^{\frac{\gamma}{2}} - Y_s^{\frac{-\gamma}{2}}}\left(\begin{array}{l} \left(\frac{r}{r_i}\right)^{\frac{-\gamma}{2}}(e-\gamma) \\ \qquad -\left(\frac{r}{r_i}\right)^{\frac{\gamma}{2}}(e+\gamma) \end{array}\right)\frac{\delta}{K} \tag{19}$$

$$\sigma_z{}^s(r) = \nu\frac{\left(\frac{r}{r_o}\right)^{\frac{e}{2}-1}}{Y_s^{\frac{\gamma}{2}} - Y_s^{\frac{-\gamma}{2}}}\left(\begin{array}{l} \left(\frac{r}{r_i}\right)^{\frac{-\gamma}{2}}\left(1+\frac{e-\gamma}{2}\right) - \\ \qquad \left(\frac{r}{r_i}\right)^{\frac{\gamma}{2}}\left(1+\frac{e+\gamma}{2}\right) \end{array}\right)\frac{\delta}{K} \tag{20}$$

For the outer cylinder $(R_i \le r \le R_0)$**,** the stress field is:

$$\sigma_r{}^c(r) = -\frac{\left(\frac{r}{R_i}\right)^{\frac{e}{2}-1}}{Y_c^{\frac{\gamma}{2}} - Y_c^{\frac{-\gamma}{2}}}\left(\left(\frac{r}{R_o}\right)^{\frac{-\gamma}{2}} - \left(\frac{r}{R_o}\right)^{\frac{\gamma}{2}}\right)\frac{\delta}{K} \tag{21}$$

$$\sigma_\theta{}^c(r) = \frac{1}{2}\frac{\left(\frac{r}{R_i}\right)^{\frac{e}{2}-1}}{Y_c^{\frac{-\gamma}{2}} - Y_c^{\frac{\gamma}{2}}}\left(\begin{array}{l} \left(\frac{r}{R_o}\right)^{\frac{-\gamma}{2}}(e-\gamma) - \\ \qquad \left(\frac{r}{R_o}\right)^{\frac{\gamma}{2}}(e+\gamma) \end{array}\right)\frac{\delta}{K} \tag{22}$$

$$\sigma_z{}^c(r) = \nu\frac{\left(\frac{r}{R_i}\right)^{\frac{e}{2}-1}}{Y_c^{\frac{-\gamma}{2}} - Y_c^{\frac{\gamma}{2}}}\left(\begin{array}{l} \left(\frac{r}{R_o}\right)^{\frac{-\gamma}{2}}\left(1+\frac{e-\gamma}{2}\right) - \\ \qquad \left(\frac{r}{R_o}\right)^{\frac{\gamma}{2}}\left(1+\frac{e+\gamma}{2}\right) \end{array}\right)\frac{\delta}{K} \tag{23}$$

The interference δ increases until it reaches the interference that causes the onset of yielding of the outer cylinder. In what follows, it is assumed that the yielding starts from the inner surface of the hollow cylinder when the interference δ_{sy} value is high.

3.2 Elastic-plastic analysis

For significantly elevated values of functionally graded materials, the initiation of yielding may emanate in either cylinders – be it the inner or outer surfaces – contingent upon the geometric and mechanical attributes of the material [20]. The yielding process commences at the inner surface of the hollow cylinder, progressively extending radially until it reaches a radius, denoted as r_c the interface radius that limits the elastic and plastic regions when the interference exceeds δ_{sy} (Figure 2).

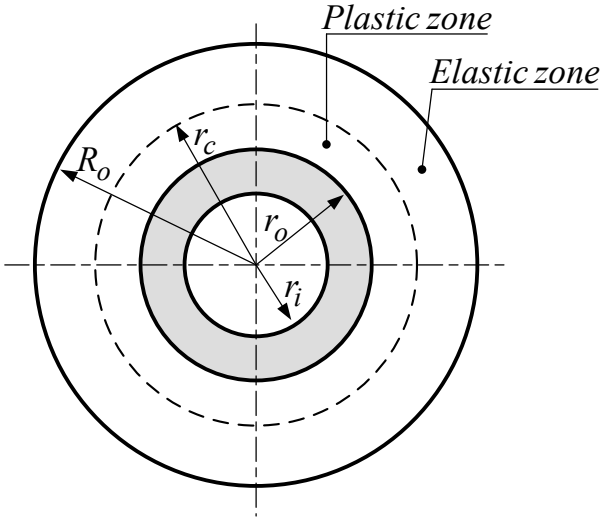

Figure 2. Shrink-fit assembly showing the outer cylinder elastic and plastic zones

3.2.1 Beginning of plasticity

The Von Mises equivalent stress is expressed as follows [21]:

$$\sigma_{eq} = \frac{\sqrt{3}}{2}\left(\sigma_\theta - \sigma_r\right) \tag{24}$$

Applying the Von Mises yield criterion at $r = R_i$

$$\sigma_{eq}(r)\Big|_{r=R_i} = \sigma_{ec}(r)\Big|_{r=R_i} \tag{25}$$

Substituting (21) and (22) into (24) and replacing r by R_i into (25) gives the pressure that starts yield in the outer cylinder:

$$P_{csyc} = \frac{2\left(1-Y_c{}^{\gamma}\right)\sigma_{oc}}{\sqrt{3}\left(\alpha Y_c{}^{\gamma}+\beta\right)} \tag{26}$$

where

$$\begin{cases} \alpha = \dfrac{e-\gamma}{2} - 1 \\ \beta = 1 - \dfrac{e+\gamma}{2} \end{cases} \tag{27}$$

The interference that starts yield in the outer cylinder is given by equating Eqs. (26) to (14)

$$\delta_{syc} = \frac{2K\left(1-Y_c{}^{\gamma}\right)\sigma_{oc}}{\sqrt{3}\ \left(\alpha Y_c{}^{\gamma}+\beta\right)} \tag{28}$$

With the interference is less then δ_{syc}, the assembly remains elastic. Above this value, the cylinder will experience partial deformation.

3.2.2 Partial plasticity

When the interference increases beyond δ_{syc}, a plastic zone of radius r_c develops. The stress-strain relationship in the plastic range is considered to follow Ludwick power law given by Eq. (6).

Under the plain strain condition $\varepsilon_z = 0$ and considering the incompressible volume assumption, it gives:

$$\varepsilon_r = -\varepsilon_\theta \tag{29}$$

Substituting Eq.(29) into the equivalent strain gives:

$$\varepsilon_{eq} = \frac{2}{\sqrt{3}}\varepsilon_\theta \tag{30}$$

The strain–displacement relations:

$$\varepsilon_r = \frac{du}{dr} \tag{31}$$

$$\varepsilon_\theta = \frac{u}{r} \tag{32}$$

Substituting (31) and (32) into (29) and integrating u_r with respect to r gives:

$$u_r = \frac{C}{r} \tag{33}$$

where u_r is the radial displacement function of the radius r and C is an integration constant.

Neglecting the body forces, the equilibrium equation of an axisymmetric problem is given by:

$$\frac{d\sigma_r}{dr} + \frac{\sigma_r - \sigma_\theta}{r} = 0 \tag{34}$$

Substituting (24) into (34) gives :

$$\frac{d\sigma_r}{dr} = \frac{2}{\sqrt{3}}\frac{\sigma_{eq}}{r} \tag{35}$$

Substituting (6) into (35) gives and integrating yields to:

$$\sigma_r(r) = \frac{2}{\sqrt{3}}\int\left(A(r) + B(r)\,\varepsilon_{eq}{}^{m}\right)\frac{dr}{r} \tag{36}$$

Combining (30), (32) and (33) gives:

$$\varepsilon_{eq}(r) = \frac{2}{\sqrt{3}}\frac{C}{r^2} \tag{37}$$

Substituting (37) and (8) into (36) and integrating gives the stresses in the plastic zone $R_i \le r \le r_0$

$$\sigma_r{}^c(r)=\frac{2}{\sqrt{3}}\left[\begin{array}{l}\dfrac{A_a}{n}\left(\dfrac{r}{R_i}\right)^n+\\ \dfrac{B_a}{k-2m}\left(\dfrac{2C_1}{\sqrt{3}R_i{}^2}\right)^m\left(\dfrac{r}{R_i}\right)^{k-2m}\end{array}\right]+C_2 \quad (38)$$

$$\sigma_\theta{}^c(r)=\frac{2}{\sqrt{3}}\left[\begin{array}{l}A_a\left(1+\dfrac{1}{n}\right)\left(\dfrac{r}{R_i}\right)^n+\\ B_a\left(\dfrac{2C_1}{\sqrt{3}R_i{}^2}\right)^m\left(1+\dfrac{1}{k-2m}\right)\left(\dfrac{r}{R_i}\right)^{k-2m}\end{array}\right]+C_2 \quad (39)$$

where C_1 and C_2 are integration constants.

By applying the Von Mises criterion at $r = r_c$, the following equations are derived.

$$\sigma_{eq}(r)\Big|_{r_c}^{elastic}=\sigma_{yc}(r)\Big|_{r=r_c} \quad (40)$$

$$\sigma_{eq}(r)\Big|_{r_c}^{plastic}=\sigma_{yc}(r)\Big|_{r=r_c} \quad (41)$$

As the plastic region reaches the radius r_c, the following boundary conditions apply.

$$\sigma_r(r)\Big|_{r=r_c}^{plastic}=\sigma_r(r)\Big|_{r=r_c}^{elastic} \quad (42)$$

The pressure at the elastic-plastic interface $r = r_c$ is defined as follows:

$$P_{r_c}=P_{r_{csyc}}\Big|_{r=r_c} \quad (43)$$

P_{r_c} $P_{r_{csyc}}$ where are the interface contact pressure and the interface contact pressure to start the yielding cylinder, respectively.

The continuity of stress at the contact hollow shaft-hollow cylinder region is expressed by (44)

$$\sigma(r)\big|_{r=R_i}=\sigma(r)\big|_{r=r_O} \quad (44)$$

The constants C_1 and C_2 are determined from previous boundary condition equations as follows :

$$C_1=\frac{R_i{}^2\sqrt{3}}{2}\left(\frac{\sigma_{oc}\left(\dfrac{r_c}{R_i}\right)^{s+2m-k}-A_a\left(\dfrac{r_c}{R_i}\right)^{n+2m-k}}{B_a}\right)^{1/m} \quad (45)$$

$$C_2=-P_{cc}-\frac{2}{\sqrt{3}}\left[\frac{A_a}{n}+\frac{1}{k-2m}\left(\begin{array}{l}\sigma_{oc}\left(\dfrac{r_c}{R_i}\right)^{s+2m-k}\\ -A_a\left(\dfrac{r_c}{R_i}\right)^{n+2m-k}\end{array}\right)\right] \quad (46)$$

By using (40) and replacing Y_c by $Y_{c_{rc}}=\dfrac{R_o}{r_c}$ and P_c by P_{r_c}, the pressure at the elastic-plastic interface is expressed as follows:

$$P_{r_c}=\frac{2\sigma_{oc}\left(1-Y_{cr_c}{}^{\gamma}\right)\left(\dfrac{r_c}{R_i}\right)^s}{\sqrt{3}\left(\alpha Y_{cr_c}{}^{\gamma}+\beta\right)} \quad (47)$$

By using (36) and (38), the residual contact pressure is expressed as follows:

$$P_{cc}=P_{r_c}-\frac{2}{\sqrt{3}}\left(\begin{array}{l}\dfrac{A_a}{n}\left(1-\left(\dfrac{r_c}{R_i}\right)^n\right)+\\ \dfrac{\sigma_{oc}\left(\dfrac{r_c}{R_i}\right)^{s+2m-k}-A_a\left(\dfrac{r_c}{R_i}\right)^{n+2m-k}}{k-2m}\times\\ \left(1-\left(\dfrac{r_c}{R_i}\right)^{k-2m}\right)\end{array}\right) \quad (48)$$

The radial stress of the elastic zone, as described by (21), is equal to the radial stress of the plastic zone, as expressed by (38), at the elastic-plastic interface radius, $r = r_c$. As a result, the numerical solution of the subsequent nonlinear equation yields the elastic-plastic interface radius, r_c:

$$\delta=\frac{r_i{}^e r_o{}^{1-e}}{Y_s{}^{\gamma}-1}\left[\frac{Y_s{}^{\gamma}}{A}-\frac{1}{B}\right]\frac{P_{cc}}{E_b}+\frac{R_i\sqrt{3}}{2}\times\left(\frac{\sigma_{oc}\left(\dfrac{r_c}{R_i}\right)^{s+2m-k}-A_a\left(\dfrac{r_c}{R_i}\right)^{n+2m-k}}{B_a}\right)^{1/m} \quad (49)$$

Substituting (45) and (46) into (38) and (39) gives the radial and hoop stresses in the plastic zone ($R_i \le r \le r_c$) as follows:

$$\sigma_r{}^c(r)=\frac{2}{\sqrt{3}}\left[\begin{array}{l}\dfrac{A_a}{n}\left(\left(\dfrac{r}{R_i}\right)^n-1\right)+\dfrac{1}{k-2m}\times\\ \left(\sigma_{oc}\left(\dfrac{r_c}{R_i}\right)^s-A_a\left(\dfrac{r_c}{R_i}\right)^n\right)\times\\ \left(\left(\dfrac{r}{R_i}\right)^{k-2m}-\left(\dfrac{r_c}{R_i}\right)^{2m-k}\right)\end{array}\right]-P_{cc} \quad (50)$$

$$\sigma_\theta{}^c(r)=\frac{2}{\sqrt{3}}\left[\begin{array}{l}\dfrac{A_a}{n}\left(\left(\dfrac{r}{R_i}\right)^n(1+n)-1\right)+\\ \left(\sigma_{oc}\left(\dfrac{r_c}{R_i}\right)^s-A_a\left(\dfrac{r_c}{R_i}\right)^n\right)\left(\dfrac{r_c}{R_i}\right)^{2m-k}\times\\ \left(\left(1+\dfrac{1}{k-2m}\right)\left(\dfrac{r}{R_i}\right)^{k-2m}-\dfrac{1}{k-2m}\right)\end{array}\right]-P_{cc} \quad (51)$$

The stresses in the elastic zone of the cylinder are determined by replacing R_i by r_c and P_c by P_{rc} in (21) and (22) (elastic zone $r_c \le r \le R_0$)

$$\sigma_r{}^c(r) = -\frac{\left(\frac{r}{r_c}\right)^{\frac{e}{2}-1}}{Y_{r_c}{}^{\frac{\gamma}{2}} - Y_{r_c}{}^{\frac{-\gamma}{2}}}\left(\left(\frac{r}{R_o}\right)^{\frac{-\gamma}{2}} - \left(\frac{r}{R_o}\right)^{\frac{\gamma}{2}}\right) \mathrm{P}_{r_c} \quad (52)$$

$$\sigma_\theta{}^c(r) = \frac{1}{2}\frac{\left(\frac{r}{r_c}\right)^{\frac{e}{2}-1}}{Y_{r_c}{}^{\frac{-\gamma}{2}} - Y_{r_c}{}^{\frac{\gamma}{2}}}\begin{pmatrix}\left(\frac{r}{R_o}\right)^{\frac{-\gamma}{2}}(e-\gamma)\\ -\left(\frac{r}{R_o}\right)^{\frac{\gamma}{2}}(e+\gamma)\end{pmatrix} \mathrm{P}_{r_c} \quad (53)$$

where $Y_{r_c} = \frac{R_o}{r_c}$ is the ratio between the outer and interface radius of the outer cylinder.

3.2.3 Plastic collapse analysis

The cylinder collapses as the interference rises and r_c equals the outer radius R_0.

At this point, the elastic zone disappears, and the hollow cylinder totally plasticizes. In this instance, assuming the radial stress indicated by (50) at the outer radius to equal zero:

$$\sigma(r)\big|_{r_c=Ro} = 0 \quad (54)$$

Replacing r_c by R_0 in (45), the integration constant becomes as follows :

$$C_{1pc} = \frac{R_i{}^2\sqrt{3}}{2}\left(\frac{\sigma_{oc}Y_c{}^{s+2m-k} - A_aY_c{}^{n+2m-k}}{B_a}\right)^{1/m} \quad (55)$$

The pressure necessary to cause the plastic collapse of the hollow cylinder, P_{spc}, is found in this instance and then expressed as follows:

$$P_{spc} = -\frac{2}{\sqrt{3}}\begin{pmatrix}\frac{A_a}{n}\left(1-Y_c{}^n\right)+\\ \frac{\left(\sigma_{oc}Y_c{}^{s+2m-k} - A_aY_c{}^{n+2m-k}\right)}{k-2m}\times\\ \left(1-Y_c{}^{k-2m}\right)\end{pmatrix} \quad (56)$$

The interference causes plastic collapse of the hollow cylinder is obtained as follows by replacing C_1 by C_{1cp} and P_C by P_{spc} in (49).

$$\delta_{spc} = \frac{R_i\sqrt{3}}{2}\left(\frac{\sigma_{oc}Y_c{}^{s+2m-k} - A_aY_c{}^{n+2m-k}}{B_a}\right)^{1/m} \quad (57)$$
$$-\frac{2}{\sqrt{3}\,E}\frac{r_i{}^e r_o{}^{1-e}}{Y_s{}^\gamma - 1}\left(\frac{Y_s{}^\gamma}{A} - \frac{1}{B}\right)\times$$
$$\begin{pmatrix}\frac{A_a}{n}\left(1-Y_c{}^n\right)+\\ \frac{\left(\sigma_{oc}Y_c{}^{s+2m-k} - A_aY_c{}^{n+2m-k}\right)\left(1-Y_c{}^{k-2m}\right)}{k-2m}\end{pmatrix}$$

4. VALIDATION USING NUMERICAL FINITE ELEMENT MODEL

The developed analytical approach was validated using the finite element model (Figure), which runs under ANSYS software. The geometrical and mechanical characteristics of the joint are shown in Table 1 below.

Table 1. Geometrical and mechanical characteristics

Outer cylinder					
R_i (mm)	R_0 (mm)	σ_{oc} (MPa)	E_0 (GPa)	s	e
40	55	400	200	2.2	3.5
A_a(MPa)	B_a(MPa)	n	k	δ (mm)	
360	480.5	2.2	2.72	0.085	
Inner cylinder					
r_i (mm)	r_0 (mm)	σ_{oc} (MPa)	E_0 (GPa)	s	e
20	40	600	200	2.2	3.5
A_a(MPa)	B_a(MPa)	n	k	δ (mm)	
360	480.5	2.2	2.72	0.085	

The inner and outer cylinders were modeled using isoperimetric 8-node plane strain elements. However, due to symmetry, only 25% of the assembly was modeled. The contact surfaces of the assembly were modeled using special contact and target elements; the friction between the mating surfaces was not taken into account because a prior study on a similar work [17] demonstrated that friction had no discernible effect on the final results. The FE model mesh refinement was validated using a mesh convergence criterion; in other words, the meshing was refined until the change in the contact pressure was less than 1%. The other parameters, like the stresses and displacements, were found to be relatively less sensitive to the mesh refinement.

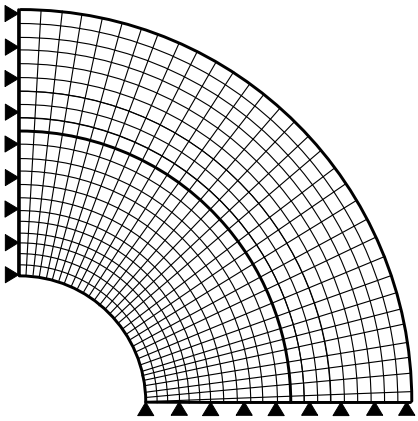

Figure 3. Finite element model in ANSYS.

5. RESULTS AND DISCUSSION

As an illustration, Figure 4 displays the variation in the elastic modulus *E(r)* as a function of radial position in the shrink-fit assembly for different values of the gradient index. The variation of these attributes can increase or decrease based on the value of the latter. When e is positive, the elastic modulus of the inner and outer hollow cylinders of the shrink-fit assembly has values that progressively increase from their inner to outer surfaces. However, with negative values of e, it decreases with the radius. Depending on the loading conditions, the value of e can be adjusted to minimize the stresses.

Figures 5 and 6 show the variation of radial, hoop, axial, and equivalent stress across the thickness of shr–ink-fit assembly for an elastic deformation ($\delta = 0.07$) and elastic-plastic deformation ($\delta = 0.084$) of the outer cylinder. It was found that a plastic zone developed from the inner surface of the outer cylinder. Therefore, the radius of plasticity depends on the value of the in–terference; it increases with the increase in the latter until the plastic collapse of the hollow cylinder is achieved.

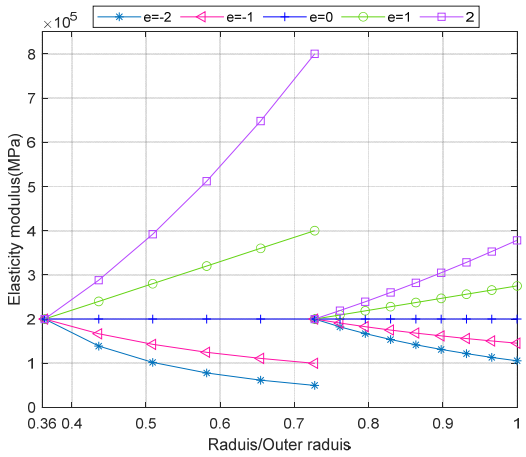

Figure 4. Variations in elasticity modulus E(r) across thickness of shrink-fit assembly for different values of gradient index e.

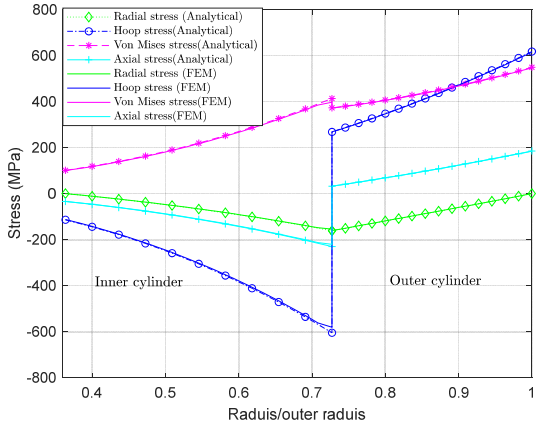

Figure 5. distribution of radial, hoop, axial, and equivalent residual stresses across the thickness of an elastically deformed shrink-fit (δ = 0.07 mm).

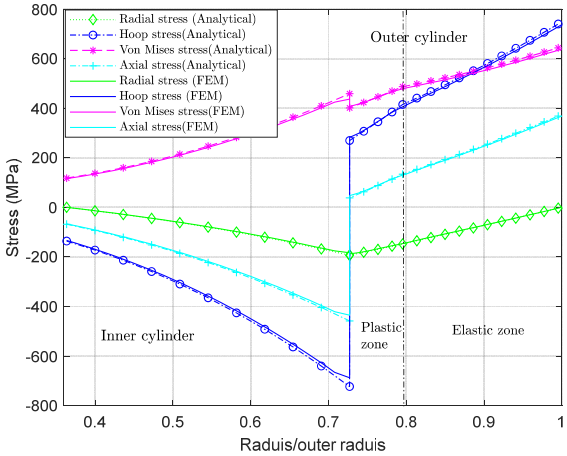

Figure 6. distribution of radial, hoop, axial, and equivalent residual stresses across thickness of an elastic-plastic shrink-fitted assembly (δ = 0.084 mm).

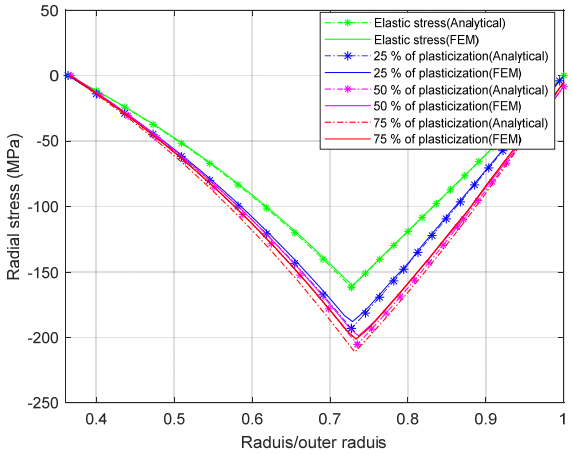

Figure 7. distribution of radial stress across the thickness of 25%, 50 % and 75% plasticized shrink-fit assembly.

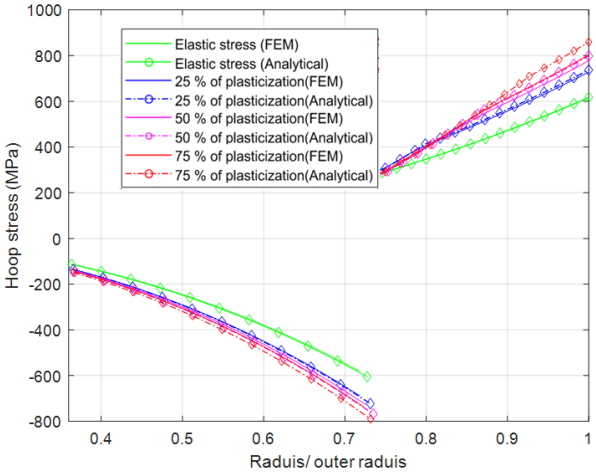

Figure 8. distribution of hoop stress across the thickness of 25%, 50 % and 75% plasticized shrink-fit assembly.

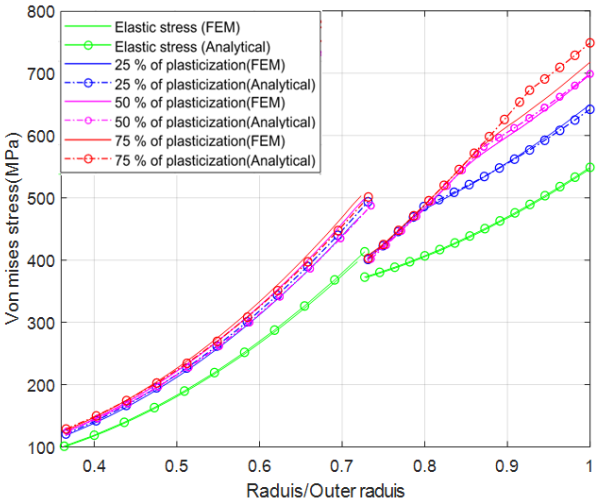

Figure 9. distribution of von mises stress across the thickness of 25%, 50 %, and 75% plasticized shrink-fit assembly.

The distributions of the radial, hoop, axial, and equi–valent stresses across the thickness of the cylinder are depicted in Figures 7–9, with the outer cylinder defor–ming plastically by 25, 50, and 75% of its thickness. The elastically deformed case is conducted with in–terference of 0.07 mm, the 25% plasticization case with 0.084 mm, the 50% plasticization case with 0.089 mm,

and the 75% plasticization case with 0.093 mm. In all cases, $e = 3.5$ and $m = 0.4$.

The radial stress exhibits an increasing trend with the rise in interference values. Consequently, there is an augmentation in the residual contact pressure at the interface, which is advantageous for efficiently transmitting substantial torque in shrink-fit assemblies. However, it is noteworthy that as the interference increases, the plastic zone of the hollow cylinder also increases. This underscores the distinctive feature of FGM materials, showcasing their adaptability to address certain challenges by adjusting mechanical and geometric characteristics to achieve desired performance outcomes.

Figure 10 illustrates the impact of the interference on the residual contact pressure for different gradient index e. As the interference increases, there is a concurrent elevation in the residual contact pressure. Additionally, it's noteworthy that the residual contact pressure increases with the increase of the gradient index.

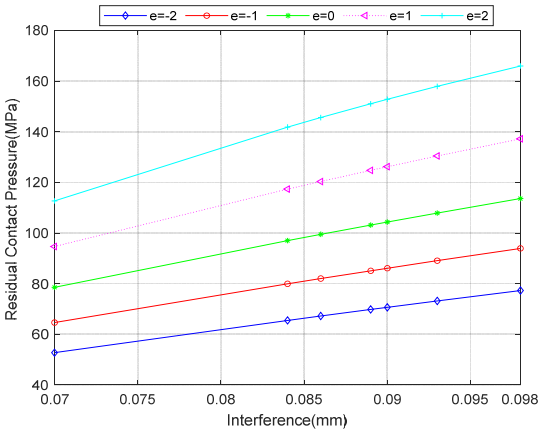

Figure 10. Influence of interference value on residual contact pressure for different values of gradient index e.

Figures 11, 12,13, and 14 show the influence of the gradient index e in the case of δ = 0.085 mm on the radial, hoop, axial, and von Mises equivalent stresses. Figure 11 displays the radial stress distribution within the shrink-fit assembly composed of Functionally Graded Materials (FGMs) cylinders, plotted against the normalized radius. The graph presents these distributions for different values of the gradient index e, with a specified interference value of 0.085 mm. Negative stress values on the graph indicate compressive residual stresses, which are typical in shrink-fit configurations due to the tight fit between inner and outer cylinders. The stress distribution is affected by the gradation in the material composition of the FGM. The value of 'e' affects the magnitude and distribution of compressive stresses due to the interference fit. A more significant gradient in material properties can lead to a more pronounced variation in stress levels. Figure 12 depicts the distribution of hoop stress within the assembly. They are significantly influenced by the non-homogeneity of the material. Higher values of 'e' might correspond to greater stiffness towards the outer radius, affecting the stress distribution accordingly.

Figure 13 depicts the axial stress distribution within a shrink-fit assembly as a function of the normalized radius for a specified interference value of 0.085 mm. The graph illustrates how different values of the gradient index e influence the axial stress within the material. The larger the e value, the more significant the deviation of the stress from zero, implying that the material's gradation has a notable impact on the axial stress levels. The effect of 'e' on the axial stress is crucial for designing FGM cylinders that can withstand specific load conditions without yielding, especially in applications where the axial load is a critical factor.

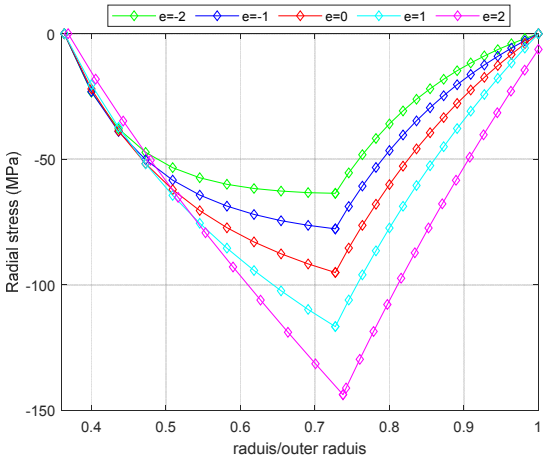

Figure 11. Radial stress distributions for different values of the gradient index e (δ = 0.085 mm)

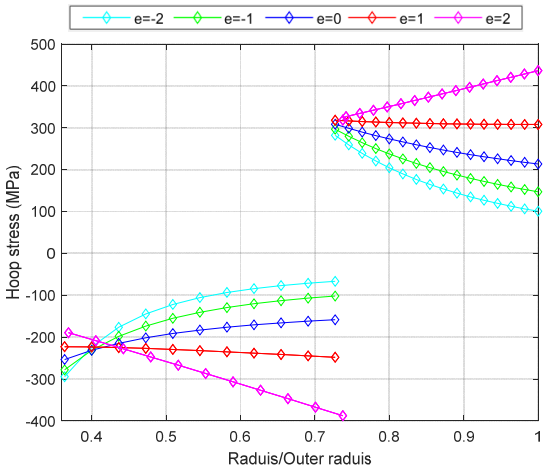

Figure 12. Hoop stress distributions for different values of the gradient index e (δ =0.085 mm).

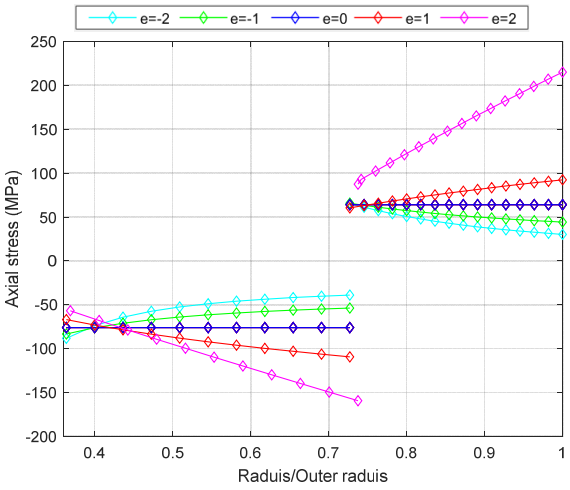

Figure 13. Axial stress distributions for different values of the gradient index e (δ = 0.085 mm)

The importance of the level of stress reached is comprehended by the equivalent stress distributed on the thickness of the inner and outer cylinders. This is depicted in Fig. 14 where the high values are located at the inner surface of the outer cylinder for all values of the gradient index.

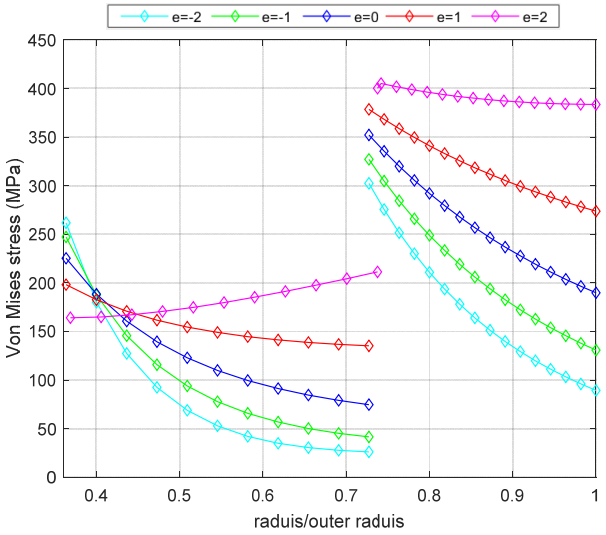

Figure 14. Von Mises equivalent stress distributions for different values of gradient index e (δ = 0.085 mm)

Figures 15 and 16 depict the influence of the Ludwik parameter 'm' on the radial and hoop stresses, considering an interference value of δ = 0.085 mm. It is evident that the radial and circumferential stresses remain unaffected by the Ludwik work-hardening exponent m of the FGM material. Consequently, it can be concluded that 'm' has an insignificant impact on the residual contact pressure.

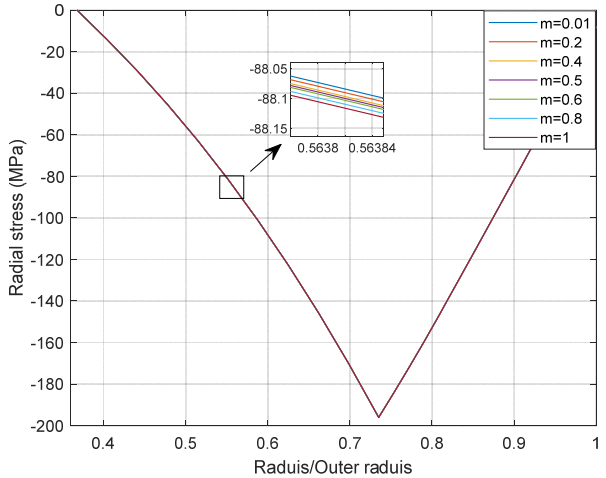

Figure 15. Radial stress distributions for different values of Ludwik parameters m (δ = 0.085 mm, e=3.5)

The impact of the gradient index e on the interference to start yield and the interference to cause plastic collapse of the outer cylinder, respectively, is depicted in Figures 17 and 18. Both interferences decrease as the gradient index increases. Table 2 shows the pressures generated at the interface by the interference that causes the start of yield and the plastic collapse of the outer cylinder for different values of the gradient index, noting that the latter is rather constant for this particular case.

In order to achieve a greater operating safety margin against yield and plastic collapse in FGM shrink-fitted assemblies, higher interference is preferable, and therefore, a low gradient index could be a solution.

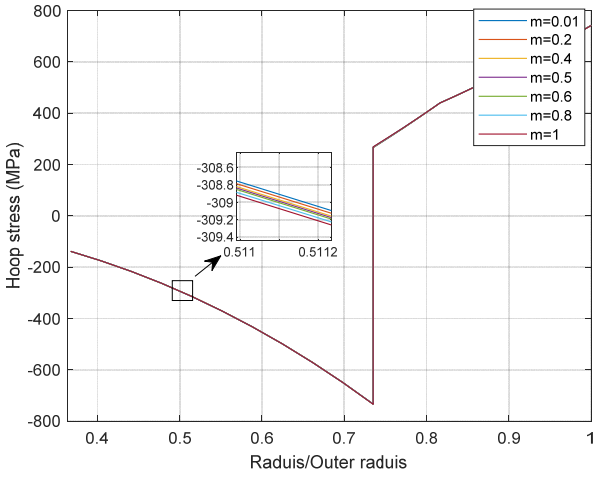

Figure 16. Hoop stress distributions for different values of Ludwik parameters m (δ = 0.085 mm, e=3,5)

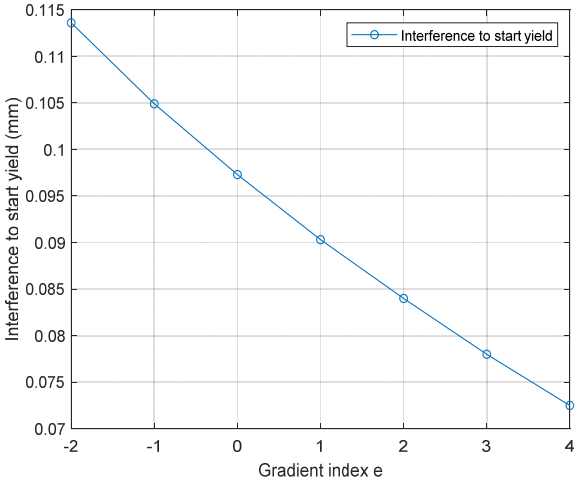

Figure 17. Interference to start yield of the outer cylinder for different values of gradient index e

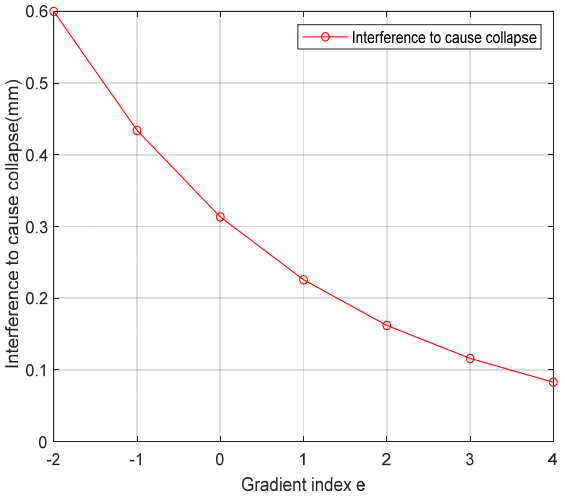

Figure 18. Interference to start the plastic collapse of the outer cylinder for different values of gradient index e

Table 2. Yield and collapse pressures of an FGM fol–low cylinder for the different values of the gradient index.

e	-2	-1	0	1	2
Start yield pressure Psy (MPa)	84.9394	95.8981	108.7900	123.9318	141.6566
Plastic col–lapse pressure Pspc (Mpa)	222.7763	220.8556	219.0909	217.4679	215.9739

6. CONCLUSION

In the realm of small deformation theory and utilizing the von Mises criteria, this article introduces analytical solutions for the elastoplastic stress behavior of a shrink-fit assembly constructed from Functionally Graded Ma–terial (FGM). Analytical and numerical methods were compared under plane strain conditions for validation purposes. The study delves into purely elastic, partially plastic, and fully plastic stress states of the assembly, exploring scenarios with a progressively increasing inter–ference value. Additionally, the article unveils the impact of both the materials and geometry on the assembly, highlighting the FGM's adaptability to meet operational requirements. The results demonstrate a noteworthy con–cordance between the analytical and simulation data.

It should be noted that the residual contact pressure increases with the increases interference value in both the elastic and plastic ranges. In addition, the residual contact pressure decreases with low values of the gra–dient index of the outer cylinder. These results provide a basis for determining the maximum allowable inter–ference to avoid adverse effects on the assembly.

This work addresses the stresses and residual contact pressure that are presented as functions of interference, which has not been addressed previously. These results provide a basis for determining the maximum allowable interference to transmit maximum torque, which is the primary purpose of shrink fitting while avoiding adverse effects on shrink-fitted assemblies.

REFERENCES

[1] Saleh, B., Jiang, J., Fathi, R., Al-hababi, T., Xu, Q., Wang, L.,... Ma, A.: 30 Years of Functionally Graded Materials: An Overview of Manufacturing Methods. Applications and Future Challenges. Composites Part B: Engineering, vol. 201, pp. 108376, 2020.

[2] Dinulović, M., Rašuo, B., Slavković, N., Karić, Đ: Analysis of Aspect and Taper Ratio on Aeroelastic Stability of Composite Shells. FME Transactions, vol. 50, no 4, pp. 732-744, 2022.

[3] Dinulović, M., Rašuo, B., Slavković, A., & Zajić, G.Flutter.: Analysis of Tapered Composite Fins: Analysis and Experiment. FME Transactions, vol 50, no 3, pp. 576-585, 2022.

[4] Dinulović, M., Rašuo, B., Trninić, M. R., Adžić, V. M.: Numerical Modeling of Nomex Honeycomb Core Composite Plates at Meso Scale Level. FME Transactions, vol. 48, no 4, pp. 874-881, 2020.

[5] Garinis, D., Dinulović, M., Rašuo, B.: Dynamic Analysis of Modified Composite Helicopter Blade. FME Transactions, vol. 40, no 2, pp. 63-68, 2012.

[6] Kumar, S., Reddy, K. M., Kumar, A., Devi, G. R.: Development and Characterization of Polymer-Ce–ramic Continuous Fiber Reinforced Functionally Graded Composites for Aerospace Application, Aerospace Science and Technology, vol. 26, no 1, pp. 185-191, 2013.

[7] Shi, Z., Zhang, T., Xiang, H.: Exact Solutions of Heterogeneous Elastic Hollow Cylinders. Compo–site structures, vol. 79, no 1, pp. 140-147, 2007.

[8] Xin, L. et al: Elastic-Plastic Analysis for Functiona-lly Graded Thick-Walled Tube Subjected to Internal Pressure. Advances in Applied Mathema-tics and Mechanics, vol. 8, no 2, pp. 331-352, 2016.

[9] Bezzie, Y. M., Woldemichael, D. E.: Investigating the Graded-Index Influence on Elastic Responses of Axisymmetric Pressurized and Heated Thick-Wal–led Functionally Graded Material of Cylindrical Ves-sel. Forces in Mechanics, vol. 7, pp. 100099, 2022.

[10] Nayak, P., Bhowmick, S., Saha, K. N: Elasto-Plas–tic Analysis of Thermo-Mechanically Loaded Fun–ctionally Graded Disks by an Iterative Variational Method. Engineering Science and Technology, an International Journal, vol. 23, no 1, pp. 42-64, 2020.

[11] Sharifi, M., Arghavani, J., Hematiyan, M. R.: An Analytical Solution for Optimum Design of Shrink-Fit Multi-Layer Compound Cylinders. International Journal of Applied Mechanics, vol. 4, no 04, pp. 1250043, 2012.

[12] Salehi Kolahi, M. R. et al.: Elastic Analysis of Shrink-Fitted Thick FGM Cylinders Based on Li-near Plane Elasticity Theory, Mech. Adv. Compos. Struct., vol. 7, no. 1, pp. 121–127, 2020.

[13] Chu, S. J., Jeong, T. K., Et Jung, E. H.: Effect of Radial Interference on Torque Capacity of Press- and Shrink-Fit Gears. International Journal of Au–tomotive Technology, vol. 17, pp. 763-768, 2016.

[14] Zhao, J. et al.: Influence of Radial Interference on Torque Capacity of Shrink-Fit Camshaft. Advances in Mechanical Engineering, vol. 11, no 4, pp. 1687814018817640, 2001.

[15] Mouaa, A. et al.: Creep Analysis of Plastically De-formed Shrink-Fitted Joints. Arabian Journal for Science and Enginee–ring, pp. 1-12, 2021.

[16] Xiang-Fa, W., Mojtaba, A., Uraching, C.: Stress Analysis of Multiple Shrink-Fitted Elastic Cylin–ders Under Thermal And Mechanical Loads. Int J. Solid Mater, vol. 1, pp. 51-77, 2019.

[17] Kazemzadeh Azad, S., Akış, T.: A Study of Shrink-Fitting for Optimal Design of Multi-Layer Compo–site Tubes Subjected to Internal and External Pressure, Iran. J. Sci. Technol. - Trans. Mech. Eng., vol. 43, pp. 451–467, 2019.

[18] Bezzie, Y. M., Woldemichael, D. E.: Effects of Graded-index and Poisson's ratio on Elastic-Solu–tions of a Pressurized Functionally Graded Material Thick-walled Cylinder. Forces in Mechanics, vol. 4, pp. 100032, 2021.

[19] Sburlati, R.: Analytical Elastic Solutions for Pres–surized Hollow Cylinders with Internal Functi–

onally Graded Coatings. Composite Structures, vol. 94, no 12, pp. 3592-3600, 2012.

[20] Atai, A. A., Lak, D.: Analytic Solution of Effect of Electric Field on Elasto-Plastic Response of a Fun–ctionally Graded Piezoelectric Hollow Cylinder. International Journal of Pressure Vessels and Piping, vol. 155, pp. 1-14, 2017.

[21] Merah, N. et al.: Finite Element Evaluation of Cle–arance Effect on Tube-to-Tubesheet Joint Strength, Int. J. Pressure Vessels Piping, vol. 80, no 12, pp. 879-885,2003.

NOMENCLATURE

r_i, r_0	Inner and outer radii of the inner cylinder (mm)
R_i, R_0	Inner and outer radii of the outer cylinder (mm)
r_c	Outer cylinder elastic-plastic interface radius (mm)
r, θ	polar coordinates
E	Young's modulus at r (MPa)
E_s	Young's modulus of the inner cylinder (MPa)
E_c	Young's modulus of the outer cylinder (MPa)
E_0	Young's modulus at $r = r_i$ and $R = R_i$, MPa
A, B	Ludwik plastic parameters at radius r, MPa
A_a, B_a	Ludwik plastic parameters at $r = r_i$, MPa
e,s,n,k	FGM gradient indexes
m	Strain hardening exponent
$Y_c = R_0/R_i$	Outer to inner radius ratio of the outer cylinder
$Y_s = r_0/r_i$	Outer to inner radius ratio of the inner cylinder
u_r	Radial displacement (mm)
P_{csyc}	The pressure that starts yield in the outer
P_i	Internal pressure (MPa)
P_c	Interface contact pressure (MPa)
P_{r_c}	Pressure at elastic-plastic interface (MPa)
$P_{r_{csyc}}$	Contact pressure that starts yield (MPa)
P_{spc}	The pressure that causes plastic collapse (MPa)
C_1, C_2, C_3	Integration constant

Greek symbols

σ_{yc}	Yield stress of outer cylinder (MPa)
σ_{ys}	Yield stress of inner cylinder (MPa)
σ_{oc}	Yield stress of outer cylinder at $r = R_i$ (MPa)
σ_{os}	Yield stress of inner cylinder at $r = r_i$ (MPa)
v	Poisson's ratio
σ_{eq}	Equivalent stress (MPa)
ε_{eq}	Equivalent strain (mm/mm)
σ_r, σ_θ, σ_z	Radial, tangential, and longitudinal stresses, respectively (MPa)
ε_r, ε_θ, ε_z	Radial, tangential, and longitudinal strains, respectively (mm/mm) δ_{syc}
δ_{syc}	Interference that starts yield (mm)
δ_{spc}	Interference that causes plastic collapse (mm)

Superscripts

s	inner cylinder
c	outer cylinder

Acronyms

FGM	Functionally Graded Material
FEM	Finite Element Method

АНАЛИЗА ЕЛАСТИЧНО-ПЛАСТИЧНОГ НАПРЕЗАЊА СКУПЉАЈУЋИХ ДЕБЕЛИХ ФГМ ЦИЛИНДАРА

С. Зринеј, Н-Е. Лагзале, А-Х.А. Бузид

Овај рад се бави анализом напрезања скупљајућих цилиндара дебелих зидова од функционално класи–фикованог материјала (ФГМ). Предложена су ана–литичка решења за еластично-пластично понашање скупљајућих осе симетричних ФГМ цилиндара де–белих зидова на основу теорије еластичности у ли–неарној равни и закона пластичности. Због функ–ционалне градације материјала, механичке карак–теристике попут Јанговог модула, напона течења и пластичних параметара контролишу се функцијом снаге дуж дебљине зида. Узимајући у обзир раван деформациони модел, еластично-савршено пластич–ни модел и Фон Мизесов критеријум приноса; добијају се теоријска решења и за еластичне и за пластичне фазе. Радијални, обруч, аксијални и екви–валентни Фон Мизесови напони се добијају за до 25%, 50% и 75% пластификације цилиндра за елас–тичне и пластичне зоне.

Напони су дати у смислу интерференције и геометријских и механичких параметара склопа. Поред тога, разматрају се смет–ње за покретање пластичне деформације и потпуни пластични колапс цилиндра. Штавише, проводе се утицај индекса градијента на контактни притисак и притисак на почетак приноса и притисак пластичног колапса. Аналитички резултати пронађени у овом истраживању упоређују се са нумеричким реше–њима које је спровео ANSYS Воркбенцх. Оба резул–тата показују добро слагање.